

# Electrochemical behavior and capacitance properties of carbon xerogel/multiwalled carbon nanotubes composites

Pablo Sebastián Fernández · Elida Beatriz Castro · Silvia Graciela Real ·  
Arnaldo Visintin · Ana Arenillas · Esther G. Calvo · Emilio J. Juárez-Pérez ·  
Angel J. Menéndez · Maria Elisa Martins

Received: 27 May 2011 / Revised: 15 June 2011 / Accepted: 20 June 2011 / Published online: 12 July 2011  
© Springer-Verlag 2011

**Abstract** The electrochemical behavior of carbon xerogel/multiwalled carbon nanotubes composite in a 6 M KOH solution has been investigated. Three different mixtures of teflonized carbons with varying nanotube content were prepared. The electrodes containing multiwalled carbon nanotubes were found to provide enhanced capacities compared with those prepared with only carbon xerogel. Cyclic voltammetry and charge–discharge experiments reveal the presence of a strong resistive component, which decreases as the amount of nanotubes increases. Electrochemical impedance spectroscopy results analyzed in terms of an adequate physicochemical model of the porous electrode, show that an increasing amount of nanotubes enhances both the effective solid-phase conductivity and the effective liquid-phase conductivity, linked to the porosity of the electrodes.

**Keywords** Electrochemical capacitors · Carbon xerogels · Carbon nanotubes · Electrochemical impedance spectroscopy

## Introduction

It is a well-known fact that energy can be stored electrostatically in electrochemical capacitors (or supercapacitors). A unit cell of an electrochemical capacitor is based on the double-layer capacitance at the solid/electrolyte interface of a high surface area material [1–6].

Electrochemical supercapacitors (ES) are extensively studied due to the increasing demand for a new kind of electrical energy accumulators with a high specific power capacity, i.e., greater than  $10 \text{ kW kg}^{-1}$  and a long durability (over  $10^6$  cycles) [1]. The main advantage of this storage system is a high dynamic of charge propagation that can be very useful for short-term pulses in hybrid electrical vehicles, digital telecommunications systems, uninterruptible power supply for computers and pulse laser technique. The development of new materials with very high specific surface areas and the use of carbons with different morphologies introduce new possibilities in a field which is in continuous progress. For this reason, the search of electrode materials suitable for electrochemical capacitors is a subject being continuously studied and developed [7–24].

Carbon gels are very interesting porous materials since their structural characteristics can be appropriately selected by choosing the right conditions for gel synthesis and processing. Carbon xerogels are frequently prepared using resorcinol (R) and formaldehyde (F) as reagents. The gel obtained is subsequently dried by evaporation and finally pyrolysed. The surfaces of RF carbon gels usually exhibit surfaces of  $600\text{--}700 \text{ m}^2 \text{ g}^{-1}$  but after being activated can exhibit surface areas higher than  $2,000 \text{ m}^2 \text{ g}^{-1}$ . Chemical activation is one of the most widely applied techniques for increasing the microporosity of carbon materials. By varying the activation conditions, it is possible to control the micropore development of carbon gels within an

---

Pablo Sebastián Fernández, Elida Beatriz Castro, Silvia Graciela Real, Arnaldo Visintin, and Maria Elisa Martins are ISE members.

P. S. Fernández (✉) · E. B. Castro · S. G. Real · A. Visintin ·  
M. E. Martins (✉)

Instituto de Investigaciones Fisicoquímicas Teóricas y Aplicadas  
(INIFTA) Facultad de Ciencias Exactas, UNLP,  
CCT La Plata-CONICET,  
1900 La Plata, Argentina  
e-mail: pfernandez@inifta.unlp.edu.ar  
e-mail: mmartins@inifta.unlp.edu.ar

A. Arenillas · E. G. Calvo · E. J. Juárez-Pérez · A. J. Menéndez  
Instituto Nacional del Carbón, CSIC,  
Apartado 73,  
33080 Oviedo, Spain

already controlled mesopore/macropore network [25–27]. The activation process allows to obtain carbons of very high surface area, although the connectivity between the carbon particles is poor, giving rise to important internal resistances. On the other hand, interesting properties are given by the presence of multiwalled carbon nanotubes (MWCNT) which exhibit a developed porosity, a high electrical conductivity and a good resilience, all being very important for enhancing the power and cycle life of supercapacitors.

In a previous article, Bordjiba et al. [28] studied the charge storage mechanism of a carbon aerogel/MWCNT composite in acid and basic medium using experimental techniques similar to those employed in the present work. However, in our electrochemical impedance spectroscopy analysis a different basic theoretical approach was followed.

The aim of this work is to provide evidence that composites formed with a very high area carbon as carbon xerogel, and MWCNT, with a good electronic conductivity, can be used to obtain a wide range of capacity–power ES. In addition, from the analysis of electrochemical measurements in terms of a dynamic physicochemical model, the factors which determine the behavior of the electrodes were identified. From a basic point of view, these studies demonstrate the improvement of the performance of the composite electrodes, due not only to the increase of the effective conductivity of the solid but also to the effective conductivity of the electrolyte within the electrode. This worthy finding is scarcely taken into account in the literature dedicated to this research field.

## Experimental

### Materials

Two different carbon materials were employed, namely, (I) MWCNT (Aldrich® Product Number 636525), with an outer diameter of 10–20 nm, an inner diameter of 5–10 nm, and a length of 0.5–200  $\mu\text{m}$ ; carbon content greater than 95%, Fe being the main impurity in the sample. Taking into account the high level of impurities, the MWCNT were purified and activated in boiling concentrated nitric acid for 2 h; (II) high specific surface area in-lab carbon xerogel (AOX). This gel was synthesized using a stoichiometric R/F molar ratio of 0.5 and a dilution ratio, D (i.e., the total solvent/reactant molar ratio), of 5.7. The initial solution had a pH of 6.5 and was placed in an oven at 85 °C for 72 h to undergo gelation and ageing. Afterwards, the aqueous gels obtained were dried by evaporation, without any pre-treatment, in the same oven at 150 °C during 24 h. The gels were then pyrolysed at 800 °C under nitrogen flow in a tubular oven, using the following heating program: (1) ramp at 1.7 °C  $\text{min}^{-1}$

to 150 °C and hold for 15 min; (2) ramp at 5 °C  $\text{min}^{-1}$  to 400 °C and hold for 60 min; (3) ramp at 5 °C  $\text{min}^{-1}$  to 800 °C and hold for 120 min; and (4) cooling slowly to room temperature. Finally, the resultant carbon xerogel was chemically activated with phosphoric acid using a mass ratio of activating agent/carbon gel of 3/1. The mixture was stirred at 85 °C for 2 h, filtered and dried overnight in an oven at 110 °C. The sample was then heated under  $\text{N}_2$  flow (85  $\text{ml min}^{-1}$ ) at 5 °C  $\text{min}^{-1}$  up to 450 °C and held at this temperature for 2 h. Finally, the samples were washed with water until pH 6 was attained and dried overnight at 110 °C.

Both carbon materials (MWCNT and AOX) were teflonized with 10 wt.% PTFE from DuPont™ Teflon® PTFE TE-3893, an aqueous dispersion fluoropolymer resin; the modified materials being named as MWCNTt and AOXt.

### Carbon characterization

The textural characterization of the samples was performed by the physical adsorption of  $\text{N}_2$  at  $-196$  °C in a TriStar II from Micromeritics. The micropore volume,  $V_{\text{DUB-N}_2}$ , was achieved by applying the Dubinin–Radushkevich (DR) method to the nitrogen adsorption isotherms [29]. The mean pore size ( $L_p$ ) was obtained from the Stoeckli equation [30], and therefore the micropore surface was then calculated ( $S_{\text{mic}}=2V_{\text{mic}}/L_p$ ). The BET surface area was also evaluated from the nitrogen adsorption isotherms [31].

The structure of the samples was evaluated by transmission electron microscopy (TEM). TEM evaluations were performed on JEOL JEM-2000 EX II equipment.

Conductivity measurements were carried out in home-made apparatus at atmospheric pressure by means of a modification of the four-point van der Pauw method [32]. For this purpose the material is pressed between two pistons and a constant current is passed through. Pressure between pistons can be controlled, a fact that allows to perform conductivity measurements in a wide pressure range. Therefore, solid conductivity of our electrodes was obtained raising the applied pressure until a constant conductivity value was reached. As it is explained in the next section, the electrodes were constructed employing the same method used to perform electrochemical measurements but without the Ni mesh.

### Electrochemical testing

In order to study their electrochemical behavior, the electrodes were prepared employing 15 mg of AOXt/MWCNTt in different ratios. These teflonized carbons were then pressed onto a nickel mesh under a pressure of 2,000  $\text{kg cm}^{-2}$  inside a 0.38  $\text{cm}^2$  transversal area cylindrical die. Three different mixtures were prepared, namely, (1) AOXt (E0), (2) AOXt with 9 wt.% of MWCNTt (E9), and (3) AOXt with 18 wt.%

of MWCNTt (E18). With the purpose of obtain well mixed carbons, the AOXt and MWCNTt materials were put in a tube with ethanol and sonicated for 15 min. The suspension was then left to dry overnight.

A three-electrode cell containing 6 M KOH was used to determine the electrochemical performance of the electrodes. The working electrode was placed between two counter-electrodes of large surface area made of a Ni mesh. The electric potentials were measured against an Hg/HgO reference electrode. Electrochemical techniques such as cyclic voltammetry (Princeton Applied Research Potentiostat/Galvanostat Model 273), galvanostatic charge and discharge experiments (Arbin Instruments model BT2000, multiple independent-channel apparatus, which operates as a potentiostat/galvanostat with charging and/or discharging capability) and electrochemical impedance spectroscopy (EIS) (frequency response analyser (FRA) Solartron 1250 and Potentiostat Model PAR 273 coupled to a PC system) were employed. All the experiments were conducted at 25 °C.

## Results and discussion

### Support characterization

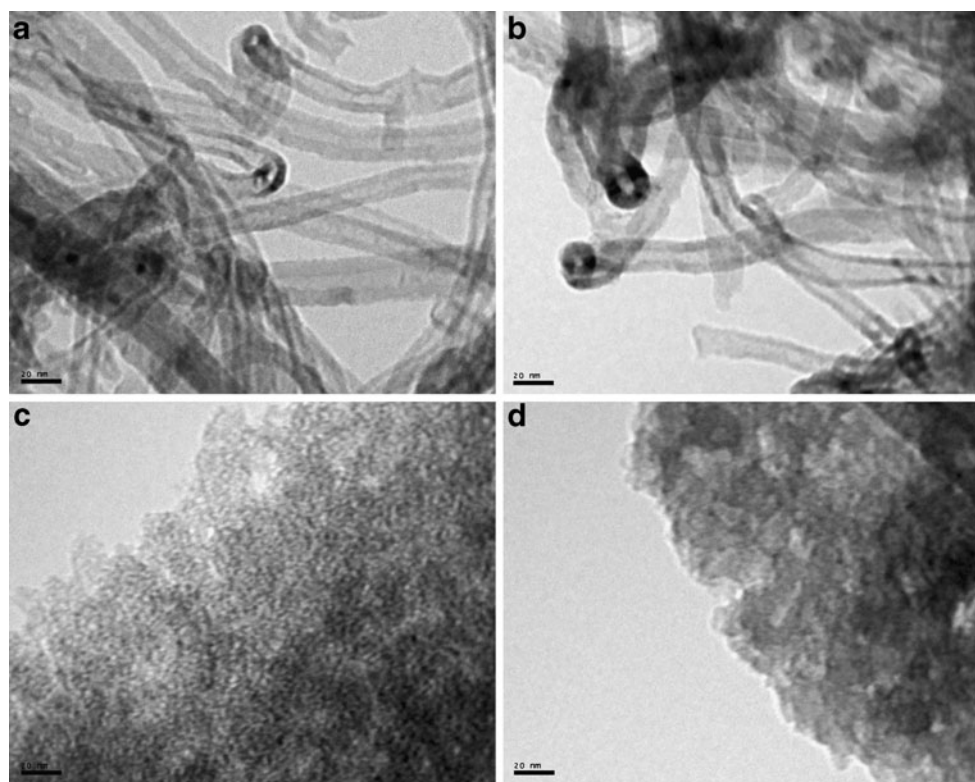
Figure 1 depicts TEM images corresponding to the studied materials. Differences in their structure can be clearly

observed. Thus, inspection of the images shows that whereas MWCNT (1a) and MWCNTt (1b) are similar, the sample AOX (1c) is different from AOXt (1d). In addition, Fig. 1a, b shows pure and homogeneous MWCNT where both the internal and outer diameter are clearly visible. Figure 1c exhibits the typical structure of an amorphous carbon in the form of carbon xerogel while in Fig. 1d, it is not possible to make out the porous structure of the gel because PTFE molecules are dispersed over the AOXt surface masking the porous structure.

TEM images corresponding to AOX-MWCNT exhibit a non homogeneous material. Thus, we have found a part of the nanocomposite containing only nanotubes; another one with only AOX; nanotubes “decorated” with AOX, and also MWCNT very well dispersed with carbon xerogel (Fig. 2).

The shape of the isotherm (Fig. 3) shows that both carbon samples (i.e., MWCNT and AOX) have very different textures. AOX is a microporous sample with a high adsorption volume at low relative pressures, while the low microporosity content in MWCNT leads to low values of adsorption. The high relative pressure part of the isotherm gives information of the presence of mesopores in the sample and their relative pore sizes. The hysteresis loop gives an approximate idea of the size and volume of the mesopores. Sample AOX has smaller mesopores (i.e., the position is at lower  $p/p^0$ ) but higher mesopore volumes (i.e., the hysteresis loop is more clearly defined). It is also

**Fig. 1** TEM images corresponding to **a** MWCNT, **b** MWCNTt, **c** AOX, and **d** AOXt



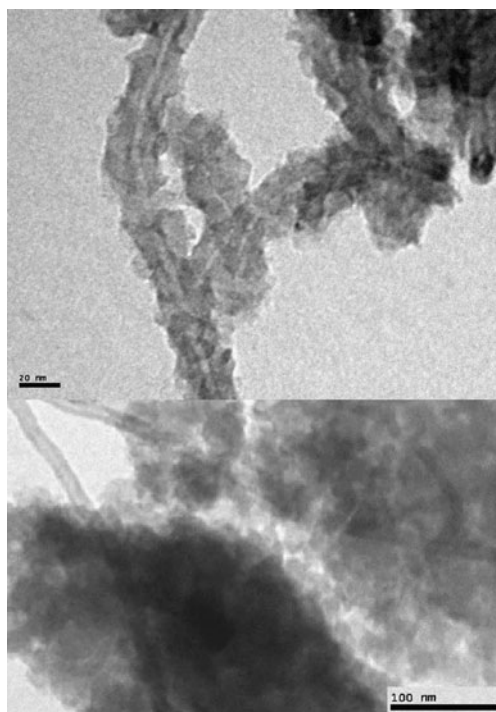


**Fig. 2** AOX-MWCNT images for MWCNT “decorated” with AOX (*upper*) and MWCNT dispersed with carbon xerogel (*lower*)

worth noting that the teflonized samples present a slightly lower development in their textural properties (i.e., lower

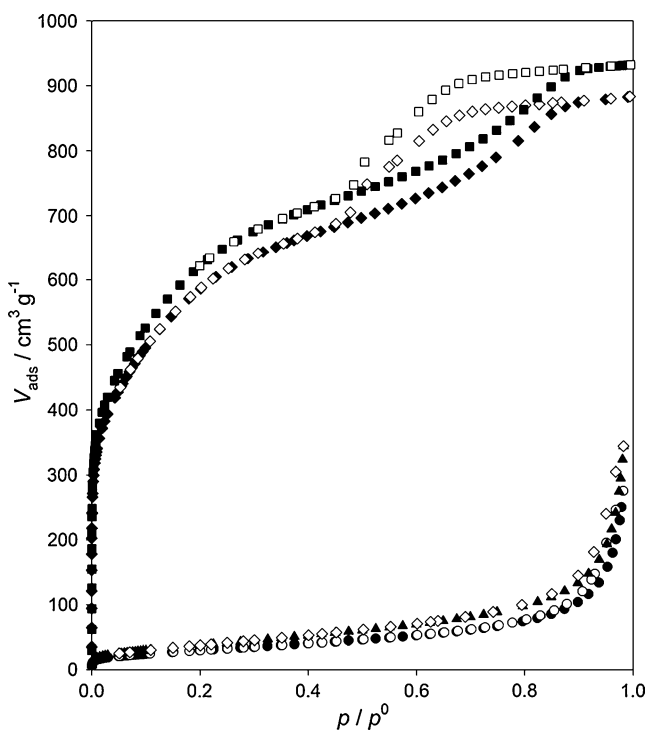


**Fig. 3** Adsorption–desorption isotherms of N<sub>2</sub> at –196 °C for: **a** MWCNT (*filled triangles*), **b** MWCNTt (*filled circles*), **c** AOX (*filled squares*), and **d** AOXt (*filled diamonds*)

surface area and porosity) than their corresponding pristine samples. A comprehensive summary of the features related to the porosity and surface areas of the carbons is presented in Table 1. As mentioned above, MWCNT has a low porosity development that is reflected in a low BET surface area, 149 m<sup>2</sup> g<sup>-1</sup>, whereas AOX has a high textural development giving a BET surface area of 2301 m<sup>2</sup> g<sup>-1</sup>, which is more than one order of magnitude higher. The values of the micropore surface and the micropore volume,  $S_{\text{mic}}$  and  $V_{\text{DUB-N}_2}$ , respectively, also differ considerably. The mean pore size  $L_p$  shows that the pores are wider in the case of MWCNT than in AOX. Comparing the textural values of the initial samples with their teflonized counterparts, it can be observed that in general the textural properties of the former are higher, although these differences are not very significant.

From results of conductivity measurements it can be concluded that an increase of nanotubes content produces an augment of material conductivity, exhibiting a linear behavior when plotted conductivity vs. MWCNT content. Thus, AOXt (E0) has a value of 0.025 S cm<sup>-1</sup> while those samples containing 9% (E9) and 18% (E18) of MWCNT have values of 0.049 and 0.115 S cm<sup>-1</sup>, respectively.

#### Electrochemical measurements

##### *Cyclic voltammetry and charge–discharge experiments*

Cyclic voltammetry (CV) was conducted performing triangular potential scans at  $\nu=1.10^{-3}$ ,  $3.10^{-3}$ ,  $5.10^{-3}$ , and  $1.10^{-2}$  V s<sup>-1</sup>. The potential routines were characterized by an upper and a lower potential limits,  $E_{\text{sa}}=-0.20$  V and  $E_{\text{sc}}=-1.10$  V, respectively.

Figure 4 exhibits voltammograms run at  $\nu=1.10^{-2}$  V s<sup>-1</sup> corresponding to all the electrodes used. The voltammograms do not exhibit the typical rectangular shape that is displayed when the electrode behaves as a pure capacitor. This behavior is due to carbon resistivity (solid and electrolyte within the porous structure), electrolyte resistance and the resistivity between carbon and current collectors. In agreement with conductivity measurements, CV results demonstrate that the resistive component increases as the amount of MWCNT decreases. Furthermore, the electrodes that contain MWCNT exhibit higher currents due to the double-layer charge–discharge.

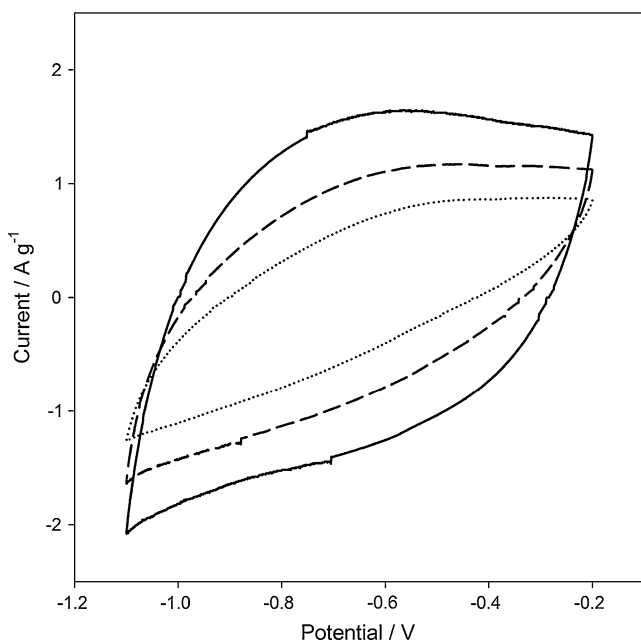
Charge–discharge (CD) measurements were performed within a potential range from –0.20 to –0.90 V. In this work, the electrodes were charged at 7.4 mA g<sup>-1</sup> and subsequently discharged at 7.4, 37.0, 74.0, and 222.0 mA g<sup>-1</sup>. These relatively low currents were selected in order to measure very high capacity values and because capacity diminishes to a great extent as the current increases.

**Table 1** Textural characteristics of the samples studied obtained from N<sub>2</sub> adsorption isotherms at -196 °C

| Sample | $S_{\text{BET}}$ (m <sup>2</sup> g <sup>-1</sup> ) | $S_{\text{mic}}$ (m <sup>2</sup> g <sup>-1</sup> ) | $V_{\text{DUB-N}_2}$ (cm <sup>3</sup> g <sup>-1</sup> ) | $L_p$ (nm) |
|--------|--|--|---|------------|
| MWCNT  | 149  | 22   | 0.04  | 3.8        |
| MWCNTt | 112  | 17   | 0.04  | 4.3        |
| AOX    | 2301   | 710  | 0.74  | 2.1        |
| AOXt   | 2158   | 711  | 0.68  | 1.9        |

Galvanostatic charge–discharge curves slightly deviate from linearity due to the occurrence of faradaic reactions. Figure 5 shows that for low current values, for instance 7.4 mA g<sup>-1</sup>, those electrodes containing MWCNTt provide enhanced capacities compared with those made up of only AOXt (E0). E18 and E9 exhibit capacity values in the order of 200 F g<sup>-1</sup> while E0 gives 176 F g<sup>-1</sup> at 7.4 mA g<sup>-1</sup>. This result implies that even at this low current not all the material responds to the current perturbation. As the current increases, the difference in capacity between E0 and E9–E18 becomes larger. Thus, while E9 and E18 have capacities of ca. 130 F g<sup>-1</sup>, E0 has a capacity of only 99 F g<sup>-1</sup>. These results indicate the existence of some overpotential, in agreement with the ohmic contribution detected in the voltammetric experiments performed with E0 electrodes.

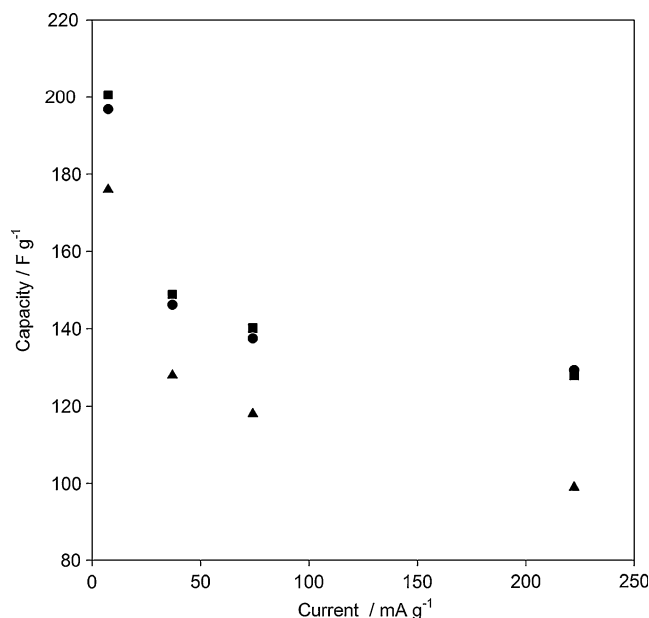
Rate capability data show that the capacity/power relationship can be set by adjusting the AOXt/MWCNTt ratio. Taking into account the behavior of E9 and E18, it is possible that the later may reach the maximum capacity that can be obtained for this order of current with the AOX-MWCNT nanocomposite.

**Fig. 4** Voltammograms of: **a** E0 (dotted line), **b** E9 (dashed line), and **c** E18 (solid line).  $E_{\text{sa}} = -0.20$  V;  $E_{\text{sc}} = -1.10$  V;  $v = 1.10 \times 10^{-2}$  V s<sup>-1</sup>; 6 M KOH;  $T = 303$  K

### Electrochemical impedance spectroscopy

Electrochemical impedance spectroscopy (EIS) measurements were carried out at -0.3 V by imposing a sinusoidal perturbation of 15 mV in the 0.5 mHz ≤  $f$  ≤ 50 kHz frequency range. The potential of -0.3 V was chosen with the aim of minimize the pseudocapacitance contribution to the electric double layer in the electrodes. This approach makes it possible to devise a simple electrochemical impedance model with the purpose of deriving the impedance function of the system and drawing direct conclusions from the fitting procedure. This topic is discussed in more detail in the next section.

The typical response of a porous electrode is shown in Fig. 6. At the highest frequencies, a semicircle whose diameter decreases as the amount of MWCNT increases can be seen. This capacitive contribution has been related to poor electrical contact between the solid particles and with the current collector (occurs because of the contact between the carbon particles and also between carbon particles and the current collector) [33]. The diameter of the semicircle decreases with the MWCNT content, probably indicating an improvement in the conductivity of the material, in

**Fig. 5** Rate capability results for E18 (filled circles), E9 (filled squares), and E0 (filled triangles). Charge current, 7.4 mA g<sup>-1</sup>

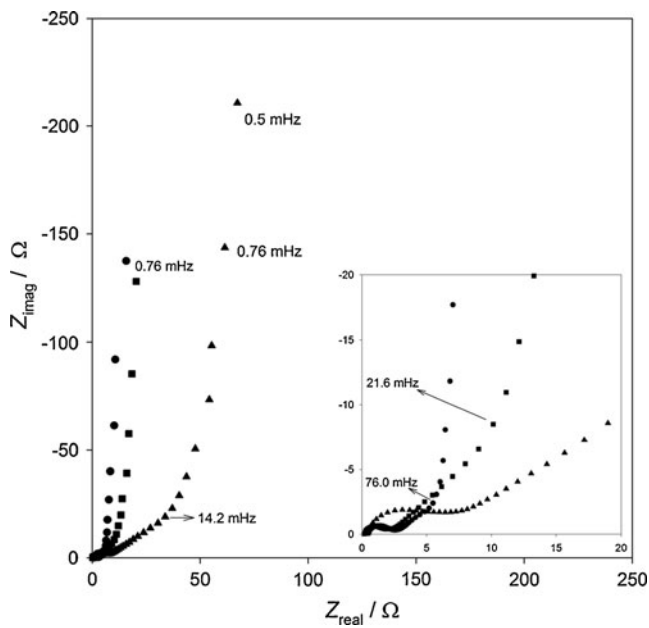


**Fig. 6** Nyquist diagrams for electrodes E18 (filled circles), E9 (filled squares), and E0 (filled triangles)

agreement with the conductivity measurements, as mentioned above. In the range of high-medium frequencies, the spectra clearly show a linear behavior with a slope of approximately  $45^\circ$ , and below a characteristic frequency, the value of the angle increases to almost  $90^\circ$ . This type of response is associated with the distribution of potential, due to finite conductivities of the electrolyte and solid phases, within the porous structure [34]. The  $45^\circ$  linear zone becomes shorter as the amount of MWCNT within the electrodes increases.

**Theoretical analysis—physicochemical model** A theoretical analysis of the dynamic electrochemical response of the system is presented and a physicochemical model is derived. In order to identify the structural and kinetic parameters of the different electrodes studied, the impedance function resulting from the model was fitted to the experimental EIS data.

The electrode is modeled as an isotropic porous structure, whose voids are filled with electrolyte. The model, based on the classic theory of porous-flooded electrodes [35, 36], takes into account the porous nature of the material, the solid and liquid conductivities, and the electrochemical processes at the solid material/electrolyte interface.

Fernández et al. carefully explain the development of this model in a previous work [37]. The final expression for the total impedance  $Z_p$  may be expressed as:

$$Z_p = \frac{L}{A_p(\kappa + \sigma)} \left[ 1 + \frac{2 + \left(\frac{\sigma}{\kappa} + \frac{\kappa}{\sigma}\right) \cosh \nu}{\nu \sinh \nu} \right] \quad (1)$$

where  $\nu$  is given by:

$$\nu = L \left( \frac{\kappa + \sigma}{\kappa \sigma} \right)^{1/2} Z_i^{-1/2}$$

$Z_i$  is the interfacial impedance per unit volume,  $A_p$  is the transverse electrode geometric area,  $L$  is the electrode thickness,  $\sigma$  is the effective carbon conductivity, and  $\kappa$  is the effective conductivity of the liquid phase.

$\kappa$  is related to the porosity ( $\varepsilon$ ) as follows,

$$\kappa = \kappa^T \varepsilon^{1.5} \quad (2)$$

where  $\kappa^T = 0.55$  is the specific conductivity ( $\Omega^{-1} \text{ cm}^{-1}$ ) of the electrolyte (6 N KOH), and the exponent, 1.5, is the tortuosity factor of the system [38, 39].

**Interfacial impedance ( $Z_i$ )** In order to calculate the total impedance  $Z_p$  using (1), an expression for  $Z_i$  ( $\Omega \text{ cm}^3$ ) is required. In our case, the interfacial impedance only implies the double-layer capacitance impedance ( $Z_{dl}$ ),

$$Z_i = Z_{dl} \quad (3)$$

where

$$Z_{dl} = \frac{1}{j\omega C_{dl}} \quad (4)$$

$C_{dl}$  is the double-layer capacitance per unit volume ( $\text{F cm}^{-3}$ );  $j$  is the imaginary number; and  $\omega = 2\pi f$  ( $f$ , frequency of the perturbing signal).

It should be pointed out that our system has two capacitances linked in parallel, namely, the double-layer capacitance and the pseudofaradaic capacitance. The latter was neglected in this model because EIS measurements were conducted at a potential value where the contribution of this capacitance to the total electrode capacity was very low.

**Results from the fitting procedure** With the aim of identify the parameters of the system, a fitting procedure of the experimental impedance data in terms of the theoretical impedance function,  $Z_p$ , was accomplished. A fitting program was developed, based on the Nelder–Meade simplex search algorithm. The fitting was considered acceptable when  $J_p$ , the cost function, is  $J_p < 5.10^{-3}$ .

$$J_p = \frac{1}{K} \sum_k \left| \frac{Z_e(\omega_k) - Z_p(p, \omega_k)}{Z_e(\omega_k)} \right|^2 \quad (5)$$

where  $K$  is the number of frequencies employed in the experiments, and  $Z_e$  and  $Z_p$  correspond to experimental and theoretical data, respectively, corresponding to the frequency  $\omega_k$ .

As contact between particles is not considered, the higher frequency values were neglected from the fitting procedure.

A comparison of the experimental results and the theoretical Nyquist diagrams derived from the fitting procedure for all the electrodes evidences a good fit (Figs. 7, 8, 9).

*Calculation and analysis of electrochemical parameters* It must be emphasized that  $a_i$ , the interfacial area per unit volume, is a parameter derived after fitting the experimental results and from the electrochemical point of view, it is a measure of the real area that takes part in the

electrode reaction. This is a point of extreme importance because the data provided by the BET method for specific area give information about the whole material used in the experiment, while the interfacial area identified from the EIS analysis, is real information about the fraction of material that actually participates in the electrode/solution interfacial process.

The capacity of the electric double-layer per electrode unit volume ( $C_{dl}$ ) is obtained from the fitting procedure for each electrode. Commonly, charge densities in the double layer at plane electrodes are in the range of  $1.6 \cdot 10^{-5}$  to  $5 \cdot 10^{-5} \text{ F cm}^{-2}$  [1]. Assuming an average value of  $3 \cdot 10^{-5} \text{ F cm}^{-2}$  ( $C_{dl}^0$ ), the interfacial area per electrode unit

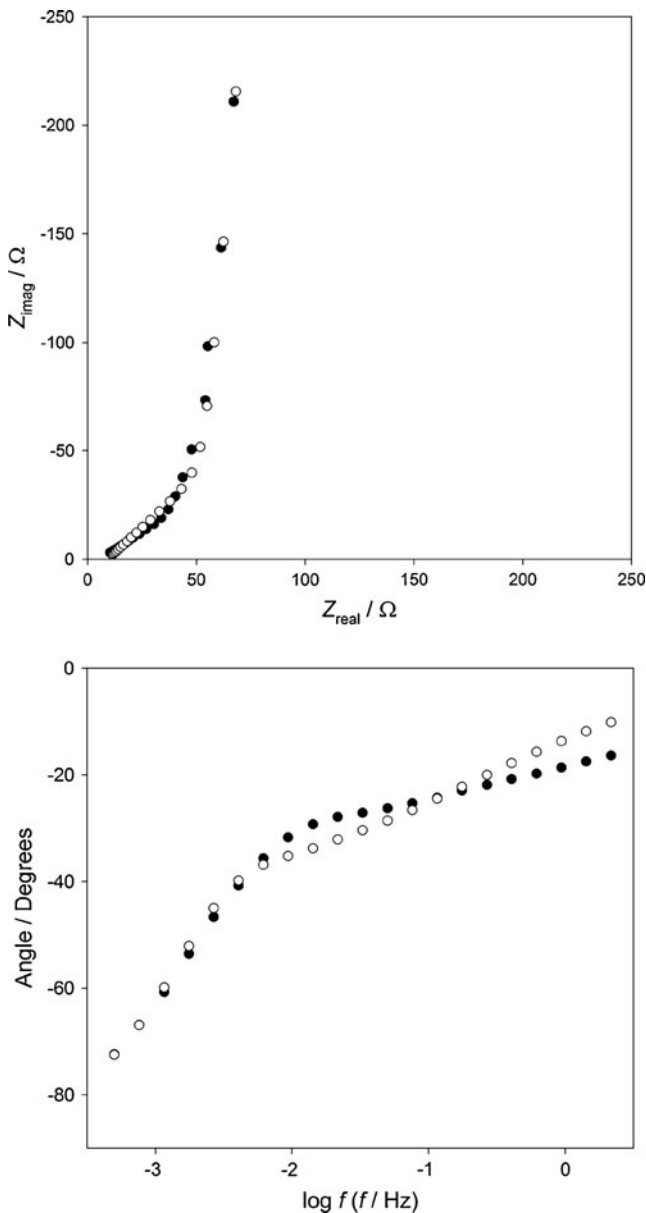


**Fig. 7** Nyquist and Bode diagrams, experimental (filled circles) and theoretical (empty circles) data, for electrode E0

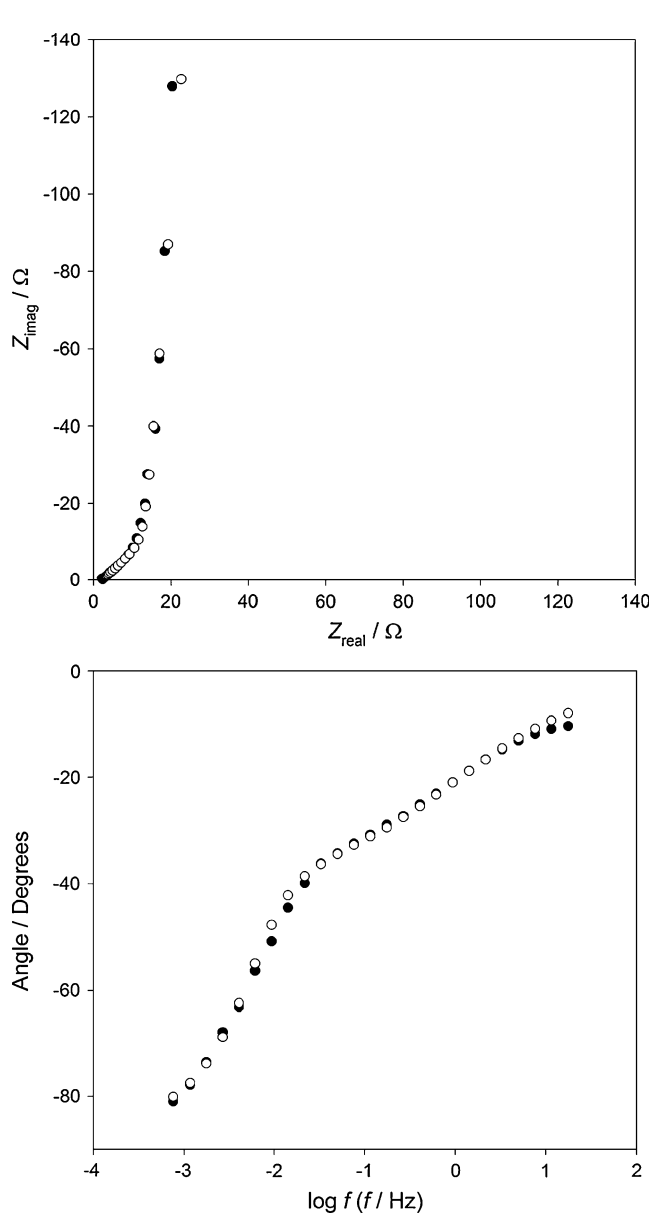


**Fig. 8** Nyquist and Bode diagrams, experimental (filled circles) and theoretical (empty circles) data, for electrode E9

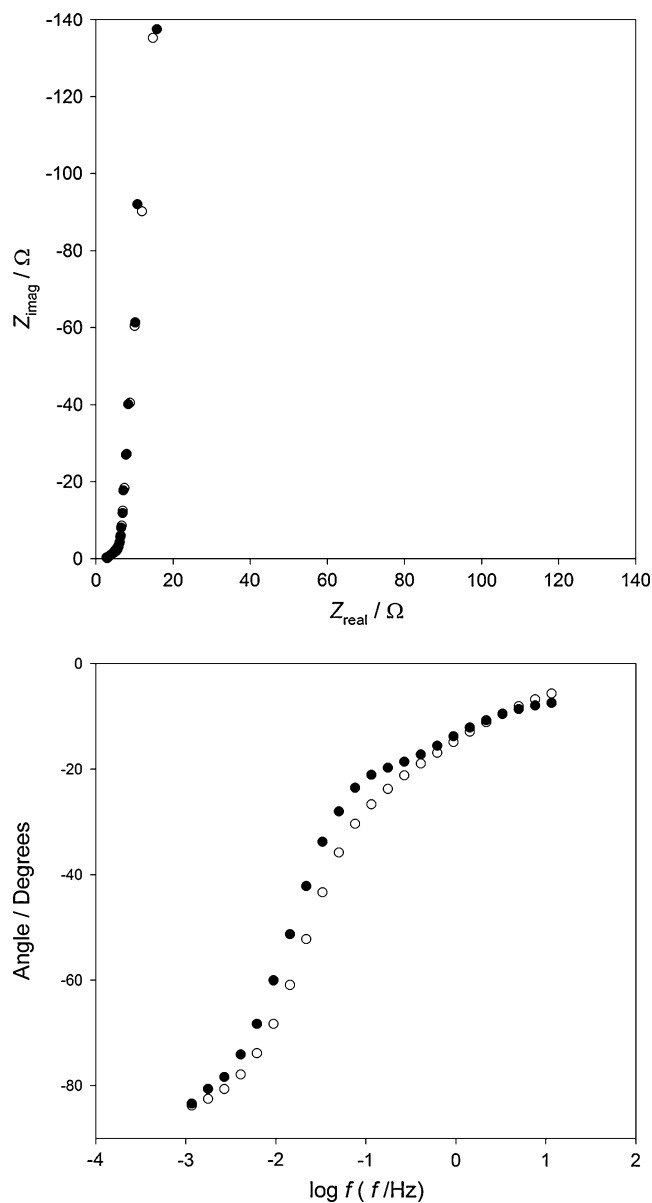


**Fig. 9** Nyquist and Bode diagrams, experimental (*filled circles*) and theoretical (*empty circles*) data, for electrode E18

volume ( $a_i$ ) for each electrode is obtained by means of the following equation,

$$C_{dl} = C_{dl}^0 a_i \quad (6)$$

Table 2 contains the model parameters derived from the fitting procedure, corresponding to electrodes of different

**Table 2** Parameters derived from the fitting procedure

| Electrode | $C_{dl}$ (F cm <sup>-3</sup> ) | $a_i$ (cm <sup>2</sup> cm <sup>-3</sup> ) | $k$ (Ω cm) <sup>-1</sup> | $C$ (F g <sup>-1</sup> ) | $S$ (m <sup>2</sup> g <sup>-1</sup> ) | $\varepsilon$ |
|-----------|--------------------------------|---|--------------------------|--------------------------|---------------------------------------|---------------|
| E18       | 39                             | 1.3·10 <sup>6</sup>                       | 0.0260                   | 110                      | 366                                   | 0.105         |
| E9        | 39                             | 1.3·10 <sup>6</sup>                       | 0.0066                   | 110                      | 366                                   | 0.052         |
| E0        | 35                             | 1.2·10 <sup>6</sup>                       | 0.0019                   | 99                       | 328                                   | 0.022         |

composition. The interfacial areas obtained from this method are quite similar for all the electrodes.

The electrochemically accessible carbon area,  $S$ , can be obtained after calculation of  $a_i$ ,

$$S = \frac{a_i \cdot V}{m} \quad (7)$$

where  $V$  is the electrode volume and  $m$  is the total carbon mass. Thus, through this parameter and by comparing with the values obtained from the BET measurements it is possible to find out the fraction of the total carbon area that is accessible to the electrolyte. From an inspection of Table 2, it is evident that  $S$  values are not so different, demonstrating that the electrolyte can gain access to almost the same fraction percentage of area in all the samples. Nevertheless, the electrodes that contain MWCNT exhibit slightly higher  $S$  values.

The most relevant differences can be found in the effective liquid-phase conductivity ( $\kappa$ ) and hence in the porosity ( $\varepsilon$ ) of the different electrodes. Percent porosity ( $\varepsilon \cdot 100$ ), obtained by using Eq. 2, increases from 2.2% for electrode E0 and reaches 10.5% for electrode E18. This enhancement of the effective liquid-phase conductivity and of the porosity of the electrodes as the amount of MWCNT increases, may account for the decrease in the resistivity component in those electrodes containing MWCNT. These data assist to understand the results obtained from the CV and CD experiments.

It must be emphasized that porosity values obtained by using BET method are different from those calculated employing electrochemical impedance results after applying the developed physicochemical model. Thus, BET results show that porosity of AOX is higher than MWCNT. Due to this fact, the porosity of the AOX/MWCNT composite will decrease as the amount of MWCNT is increased. Furthermore, it must be taken into account that in contrast to BET method where the porosity of the material depends on the amount of nitrogen incoming within the pores, in the electrochemical method the results of porosity values are obtained through a physicochemical model. In the latter method, the porosity of the material is measured or sensed through the electrolyte incoming inside the pores of the electrode, which in turn is responsible of the electric conductivity. From these results, it can be concluded that this carbon xerogel is not good enough as material for supercapacitor due to its pores size distribution that



impedes that a great part of the micropores could be occupied by the electrolyte.

This fact explains why  $C_{dl}$  does not decrease when the amount of MWCNT is increased. Even though the surface area calculated with BET method decreases with the increment of MWCNT, on the other hand, the accessibility of the electrolyte within the porous structure enhances.

For the reasons exposed above, we consider necessary to improve the xerogel synthesis to achieve a better pore distribution with the aim to get higher accessibility of the electrolyte inside the porous material and having enhanced effective liquid-phase conductivity. At the present, we are working on the synthesis of carbons xerogels with a larger mesopore/micropore ratio.

## Conclusions

The voltammetric results demonstrate that there is an important resistive component which increases as the amount of MWCNT decreases. Furthermore, those electrodes containing MWCNT exhibit higher currents related to the double-layer charge–discharge mechanism. These results can be attributed to an increase in the electronic conductivity of the solid phase, and, according to the impedance fitting procedure, to an increase in the effective conductivity of the liquid phase as the amount of MWCNT augments.

The rate capability data show that the capacity/power relationship in the capacitor can be set by adjusting the AOXt/MWCNTt ratio. In addition, taking into account the behavior of E9 and E18, it is possible that E18 comes close to reaching the maximum capacity that can be obtained for this order of current with the AOX-MWCNT nanocomposite.

Conductivity measurements and EIS results demonstrate that electrode conductivity is increased by adding MWCNT. This is clearly seen at the highest frequencies in the Nyquist diagram. The decrease in the diameter of the semicircles is attributed to a better conductivity in the carbon materials.

On a basis of a theoretical analysis of the dynamic electrochemical response of the system a physicochemical model has been derived. In order to identify the structural and kinetic parameters of the different electrodes studied, theoretical impedance was fitted to the experimental data. The interfacial areas obtained through this method are slightly similar for all electrodes, demonstrating that the electrolyte can gain access to the same percentage of area in all of the samples tested.

The fitting procedure applied contributed significantly to understand the results found in both the CV and CD experiments. It was found that as the amount of MWCNT

increases, an enhancement of effective liquid-phase conductivity associated to a higher porosity of the electrodes occurs. This fact, in addition to the effective solid electric conductivity, accounts for the decrease in the resistive component of those electrodes that contain MWCNT.

**Acknowledgments** This work was supported by the Consejo Nacional de Investigaciones Científicas y Técnicas of Argentina, the Agencia Nacional de Promoción Científica y Tecnológica, and the Universidad Nacional de La Plata. The financial support received from the Government of Principado de Asturias PCTI (Ref. IB09-00201) and Ministerio de Ciencia e Innovación (Ref. MAT2008-00217/MAT) is also greatly acknowledged. E.G. Calvo also acknowledges a predoctoral research grant from FICYT.

## References

1. Conway BE (1999) *Electrochemical supercapacitors, scientific fundamentals and technological applications*. Plenum, New York
2. Conway BE (1991) Transition from “supercapacitor” to “battery” behaviour in electrochemical energy storage. *J Electrochem Soc* 138:1539–1548
3. Sarangapani S, Tilak BV, Chen CP (1996) Materials for electrochemical capacitors. *J Electrochem Soc* 143:3791–3799
4. Burke A (2000) Ultracapacitors: why, how, and where is the technology. *J Power Sources* 91:37–50
5. Conway BE, Birss V, Wojtowicz J (1997) The role and utilization of pseudocapacitance for energy storage by supercapacitors. *J Power Sources* 66:1–14
6. Frackowiak E, Béguin F (2001) Carbon materials for the electrochemical storage of energy in capacitors. *Carbon* 39:937–950
7. Béguin F (2006) Application of nanotextured carbons for electrochemical energy storage in aqueous medium. *J Braz Chem Soc* 17:1083–1089
8. Qu D, Shi H (1998) Studies of activated carbons used in double-layer capacitors. *J Power Sources* 74:99–107
9. Björnbohm P (2007) Charge/discharge of an electrochemical supercapacitor electrode pore; non-uniqueness of mathematical models. *Electrochem Commun* 9:211–215
10. Frackowiak E, Jurewicz K, Szostak K, Delpeux S, Béguin F (2002) Nanotubular materials as electrodes for supercapacitors. *Fuel Process Technol* 77–78:213–219
11. Jurewicz K, Vix-Guterl C, Frackowiak E, Saadallah S, Reda M, Parmentier J, Patarin J, Béguin F (2004) Capacitance properties of ordered porous carbon materials prepared by a templating procedure. *J Phys Chem Solids* 65:287–293
12. Sullivan MG, Schnyder B, Bärtsch M, Alliata D, Barbero C, Imhof R, Kötz R (2000) Electrochemically modified glassy carbon for capacitor electrodes. Characterization of thick anodic layers by cyclic voltammetry, differential electrochemical mass spectrometry, spectroscopic ellipsometry, X-ray photoelectron spectroscopy, FTIR, and AFM. *J Electrochem Soc* 147:2636–2643
13. Vix-Guterl C, Frackowiak E, Jurewicz K, Friebe M, Parmentier J, Béguin F (2005) Electrochemical energy storage in ordered porous carbon materials. *Carbon* 43:1293–1302
14. Barbieri O, Hahn V, Herzog A, Kötz R (2005) Capacitance limits of high surface area activated carbons for double layer capacitors. *Carbon* 43:1303–1310
15. Lota G, Grzyb B, Machnikowska H, Machnikowski J, Frackowiak E (2005) Effect of nitrogen in carbon electrode on the supercapacitor performance. *Chem Phys Lett* 404:53–58

16. Planes GA, Miras MC, Barbero CA (2005) Double layer properties of carbon aerogel electrodes measured by probe beam deflection and AC impedance techniques. *Chem Commun* 16:2146–2148
17. Raymundo-Piñero E, Leroux F, Béguin F (2006) A high-performance carbon for supercapacitors obtained by carbonization of a seaweed biopolymer. *Adv Mater* 18:1877–1882
18. Kim JH, Nam K-W, Ma SB, Kim KB (2006) Fabrication and electrochemical properties of carbon nanotube film electrodes. *Carbon* 44:1963–1968
19. Cebeci FÇ, Sezer E, Sarac AS (2009) A novel EDOT–nonylbithiazole–EDOT based comonomer as an active electrode material for supercapacitor applications. *Electrochim Acta* 54:6354–6360
20. Niu C, Sichel EK, Hoch R, Moy D, Tennent H (1997) High power electrochemical capacitors based on carbon nanotube electrodes. *Appl Phys Lett* 70:1480–1482
21. Vix-Guterl C, Saadallah S, Jurewicz K, Frackowiak E, Reda M, Parmentier J et al (2004) Supercapacitor electrodes from new ordered porous carbon materials obtained by a templating procedure. *Mat Sci Eng B* 108:148–155
22. Malak A, Fic K, Lota G, Vix-Guterl C, Frackowiak E (2010) Hybrid materials for supercapacitor application. *J Solid State Electrochem* 14:811–816
23. Zhongxue L, Jie C (2008) An impedance-based approach to predict the state-of-charge for carbon-based supercapacitors. *Microelectron Eng* 85:1549–1554
24. Simon P, Gogotsi Y (2008) Materials for electrochemical capacitors. *Nat Mater* 7:845–854
25. Zubizarreta L, Arenillas A, Pis JJ, Pirard V, Job N (2009) Studying chemical activation in carbon xerogels. *J Mater Sci* 44:6583–6590
26. Stoeckli F, Centeno TA (2005) On the determination of surface areas in activated carbons. *Carbon* 43:1184–1190
27. Dubinin MM (1966) Porous structure and adsorption properties of active carbons. In: Walker PL Jr (ed) *Chemistry and physics of carbon*, vol 2. Marcel Dekker, New York, pp 51–120
28. Bordjiba T, Mohamedi M, Dao LH (2008) Charge storage mechanism of binderless nanocomposite electrodes formed by dispersion of CNTs and carbon aerogels. *J Electrochem Soc* 155: A115–A124
29. Dubinin MM (1975) In: Danielli JF, Rosenberg MD, Cadenhead D (eds) *Progress in surface and membrane science*, vol 9. Academic, New York
30. Stoeckli HF, Ballerini L (1991) Evolution of microporosity during activation of carbon. *Fuel* 70:557–560
31. Parra JB, de Sousa JC, Bansal RC, Pis JJ, Pajares JA (1995) Characterization of activated carbons by the BET equation—an alternative approach. *Adsorpt Sci Technol* 12:51–66
32. van der Pauw J (1958) A method of measuring specific resistivity and Hall effect of discs of arbitrary shape. *Philips Res Repts* 13:1–9
33. Lundqvist A, Lindbergh G (1999) Kinetic study of a porous metal hydride electrode. *Electrochim Acta* 44:2523–2542
34. de Levie R (1963) On porous electrodes in electrolyte solutions. *Electrochim Acta* 8:751–780
35. Castro EB, Real SG, Bonesi A, Visintin A, Triaca WE (2004) Electrochemical impedance characterization of porous metal hydride electrodes. *Electrochim Acta* 49:3879–3890
36. Meyers JP, Doyle M, Darling RM, Newman JJ (2000) The impedance response of a porous electrode composed of intercalation particles. *J Electrochem Soc* 147:2930–2940
37. Fernández PS, Castro EB, Real SG, Martins ME (2009) Electrochemical behaviour of single walled carbon nanotubes—hydrogen storage and hydrogen evolution reaction. *Int J Hydrogen Energy* 34:8115–8126
38. De Vidts P, White RE (1995) Mathematical modeling of a nickel-cadmium cell: proton diffusion in the nickel electrode. *J Electrochem Soc* 142:1509–1519
39. Shung-Ik L, Yun-Sung K, Hai-Soo C (2002) Modeling on lithium insertion of porous carbon electrodes. *Electrochim Acta* 47:1055–1067